Electrical properties of $Pb(Mn_{1/3}Nb_{2/3})O_3$ ceramics under hydrostatic pressure: Relaxation dynamics and its relation to the subsystem of defects

Andrzej Molak,* Marian Paluch, and Sebastian Pawlus
Institute of Physics, University of Silesia, ul. Uniwersytecka 4, 40-007 Katowice, Poland
(Received 3 April 2007; revised manuscript received 4 August 2008; published 30 October 2008)

The dynamics of electrical conduction relaxation has been studied for the disordered $Pb(Mn_{1/3}Nb_{2/3})O_3$ ceramics. Broadband dielectric spectroscopy at frequency $f=10^{-1}-10^{7}$ Hz was applied within the temperature range 173–473 K. The real ε' and imagimary ε'' parts of complex dielectric permittivity at isothermal and isobaric thermodynamic conditions were measured. The hydrostatic pressure was changed up to 1.76 GPa. Two relaxation mechanisms were discerned. The isotherm has been fitted to activation law, $\tau(p)=\tau_0 \exp[p\Delta V_a/RT_{\mathrm{iso}}]$ above and below a crossover pressure $p_{\mathrm{cr}}\approx 0.9$ GPa. The temperature dependence of relaxation times scales to the thermally activated electric conductivity, $\sigma(0,T)\sim 1/\tau_m$ in the high-temperature range. The applied hydrostatic pressure decreased activation energies and stabilized the Fermi-glass features. The pressure effects have been discussed in framework of the Gate model, focused on the bivacancies' role in the strain-related activation energy.

DOI: 10.1103/PhysRevB.78.134207 PACS number(s): 61.50.Ks, 72.20.Ee, 75.47.Lx, 77.22.Gm

I. INTRODUCTION

Both dipolar and/or electric conductivity relaxation processes are usually observed in the disordered solids and the latter may be related either to crystal lattice or to defects subsystem response. The interaction of electric dipolelike defects with neighborhood results in the non-Debye character of response of investigated material.[1] Consequently, in many cases the Arrhenius law cannot describe satisfactorily the temperature relaxation dynamics of disordered materials. For instance the non-Arrhenius behavior of a structural relaxation is commonly observed in variety of disordered systems like glass-forming liquids,[2] polymers,[3] relaxors,[4–6] and dipolar glasslike states[7,8] where the Vogel-Fulcher-Tamann (VFT) law[9] is usually applied for the analysis of temperature dependence of structural relaxation times. However, the relaxation dynamics of the mentioned above materials could be changed not only by temperature but also by applied pressure. In such case, pressure dependence of the structural relaxation could not be described exactly also by the activation law.[10]

The oxide perovskites are the materials that exhibit sensitivity of electrical and structural properties on hydrostatic pressure. Hydrostatic pressure affects primarily dynamics of atoms in the crystal lattice and it is known that the structural phase transitions are influenced by pressure.[11–14]

It is expected that in the case when the crystal structure is involved in the relaxation process, the electric response of the system can be pressure dependent due to electron-lattice coupling. In case of mixed ionic-electronic conduction both ionic and electronic effects may manifest in the response to the applied fields. Participation of vacancies in the electric conduction and relaxation phenomena is generally accepted since they offer facilities for the hopping of ions at temperatures high enough. They also serve as the source of thermally generated electrons for conduction. The decrease in the ion spacing and/or decrease in the jump distance between the sites in the crystal lattice, caused by application of the hydrostatic pressure, can result in a decrease in the energy barrier height.[15,16] Hence, the results obtained from the electrical measurement carried out under elevated pressure may provide insight into structural effects in the electrical relaxation phenomena in the perovskites. Such studies can be interesting since the relaxation dynamics becomes an important factor in the electromechanic behavior of perovskite materials.

Surprisingly, several materials, which show not only structural relaxation phenomena but also high electric conduction, exhibit another type of temperature dependence of relaxation times. Such behavior can be detected also in many ceramics materials. When the relaxation times of electric conductivity scale with the dc electric conductivity temperature dependence, the relation known as the "conduction current relaxation" term $\sigma_{\mathrm{dc}}=\xi/\tau$ (the B-N-N relation)[17] is fulfilled. Hence, when the electrons are localized in the vicinity of the Fermi level and they form the Fermi glass, the conductivity is commonly described within the variable range hopping (VRH) of small polaron model of conductivity, i.e., $\sigma_{\mathrm{dc}}\propto\exp[-(T_0/T)^p]$, where $p=1/2$, 1/3, or 1/4, in accordance to dimensionality of the subsystem where the electric conduction proceeds. Therefore, the temperature dependence of relaxation times τ_m exhibits also the non-Arrhenius behavior, in accordance with expression $\ln\tau_m\sim(T_0/T)^p$.[18]

For instance, several perovskites containing manganese ions show conduction consistent with the VRH model in low-temperature range, $\ln\sigma\sim-(T_0/T)^p$, and the Fermi-glass features are deduced from the scaling "conduction current relaxation" term. This type of conduction is not limited to a particular group of manganites,[19–21] but occurs for a variety of materials and different temperature ranges.[22–26]

Recently, the electric properties of the complex perovskite systems with admixture of $Pb(Mn_yNb_{1-y})O_3$ ceramics were investigated.[27–30] It was shown that such manganite-niobate-based compounds, e.g., $Pb(Mg_{1/4}Mn_{1/4}Nb_{1/2})O_3$,[30] $Pb(Mn_{1/3}Nb_{2/3})O_3$-$Pb(ZrTi)O_3$,[31,32] $Pb(Mn_{1/3}Nb_{2/3})O_3$-$Pb(MgNb)O_3$-$Pb(ZrTi)O_3$,[33] $Pb(Mn_{1/3}Nb_{2/3})O_3$-$Pb(MgNb)O_3$-$PbTiO_3$,[34] and $BiScO_3$-$PbTiO_3$-$Pb(Mn_{1/3}Nb_{2/3})O_3$,[35] exhibit electrical properties suitable for

electromechanical applications. It was also found that the doping with acceptor Mn ions replacing Nb improves, e.g., the mechanical quality factor Q_m of such solid solutions.[31–35] It was pointed out that the doping with heterovalence Mn ions may facilitate the formation of electric dipoles[31] that leads, in consequence, to the appearance of electric relaxation phenomena.

The better understanding of the phenomena mentioned above can be, undoubtedly, achieved by studying the electrical properties of the $Pb(Mn_{1/3}Nb_{2/3})O_3$ material under high-pressure conditions. It should be emphasized that the studied $Pb(Mn_{1/3}Nb_{2/3})O_3$ compound despite the formal $A(B'_{1/3}B''_{2/3})O_3$ composition does not show features typical for the conventional relaxors or ferroelectrics with diffused phase transition. Its properties, despite the speculative similarity of the $\varepsilon'(f,T)$ shape to those of relaxor type, are basically different due to fact that the electric permittivity $\varepsilon'(T)$ of the $Pb(Mn_{1/3}Nb_{2/3})O_3$ shows moderate value $\varepsilon'_{max} \approx 1000$ in the peak maximum. Moreover, the position of the peak in $\varepsilon'(T)$ markedly depends on frequency and the shift of the peak occur within a wide range from 350 to 650 K when measured in frequency range 100 Hz–100 kHz.[4,6,7,12,29,36] Furthermore, the behavior of dispersion phenomenon in the studied $Pb(Mn_{1/3}Nb_{2/3})O_3$ ceramics was ascribed to the relaxation of electric current conduction[29] but not to the relaxation of polar nanoregions. The values of the characteristic times of electric conductivity relaxation and the corresponding activation energy indicated an ionic mechanism of this relaxation. The former analysis suggested that both the Mn doping ions and the oxygen vacancies, forming Mn-V_O complexes, were responsible for the relaxation phenomena. The minor frequency-dependent anomaly was related to the other polaronic conduction relaxation occurring within 170–250 K range. Moreover, it was deduced from semiconductor properties that mixed ionic and polaronic conduction participates in the relaxation that correlated with the locally disordered crystal lattice.[29]

Herein we present the results of investigation of the electrical properties of the $Pb(Mn_{1/3}Nb_{2/3})O_3$ ceramics under hydrostatic pressure at isothermal and isobaric conditions. Dielectric spectroscopy results enabled us to analyze the conduction mechanism involved in relaxation. We discerned whether and when the ionic or polaronic component dominated in the electric relaxation of the studied $Pb(Mn_{1/3}Nb_{2/3})O_3$ material.

II. EXPERIMENT

The $Pb(Mn_{1/3}Nb_{2/3})O_3$ ceramics have been obtained by dry sintering. Long-term milling was applied for mixing the powders. X-ray diffraction (XRD) pattern analysis showed that the main phase (>91%) has the perovskite-derived monoclinic symmetry and the deformed, multiple unit cell parameters were determined: $a=12.193$ Å, $b=11.966$ Å, $c=12.144$ Å, and $\beta=90°10.7'$.[29] The scanning electron microscopy (SEM) test confirmed this result, showing composition close to nominal perovskite for the main phase, although a variance in the chemical composition for particular grains occurred. A minor phase with another chemical composition and precipitation of MnO_2 were also found.[29] The $Pb(Mn_{1/3}Nb_{2/3})O_3$ sample for the dielectric measurement was cut from the sintered ceramics pellet, polished and sputtered with (~80 nm) Au electrodes. Dielectric measurements were carried out in a frequency range from 10^{-1} to 10^7 Hz using a Novocontrol Alpha Impedance Analyzer. The sample was placed in a Teflon bellows filled with silicon oil and mounted in the high-pressure chamber. Displacing the piston by means of a hydraulic press generated the hydrostatic pressure.[10] The pressure was changed up to 1.76 GPa in case of the isothermal measurement carried out at $T_{iso}=272$ K. At the isobaric conditions, the measurement was carried out at $p=1.76$ GPa and the temperature was changed within the 252–366 K range, with a step of 5 K and at each temperature stabilization time was 10 min.

The effective Young's modulus value $C=117$ Pa, needed for necessary numerical evaluations, has been taken as the value measured for the other ceramic sample compound with similar composition, however with the same Mn:Nb concentration. The $C=116.8\pm9.5$ GPa value has been obtained in nanoindentation test carried out in Hysitron Laboratory for $Bi(Mn_{1/3}Nb_{2/3})O_3$ ceramic compound.

III. RESULTS

A. Relaxation processes at ambient pressure

Structural properties (XRD), chemical composition (SEM, EPMA), and results of electric measurements of $Pb(Mn_{1/3}Nb_{2/3})O_3$ ceramics at ambient pressure were reported in our previous article.[29] The relaxation processes were partially covered by the electric conduction.

The $Pb(Mn_{1/3}Nb_{2/3})O_3$ samples showed the marked electric conductivity which varied from $\sim 10^{-10}$ S m^{-1} at $T=100$ K up to ~0.2 S m^{-1} at $T=700$ K. It showed dispersion and thermally activated dependence described with formula

$$\sigma(f,T) = \sigma_{dc} + A\omega^S \tag{1a}$$

with direct current conductivity part

$$\sigma_{dc} = \sigma_{0,dc} \exp[-(E_{dc}/k_B T)]. \tag{1b}$$

The activation energy $E_{dc}=0.45$ eV was determined above $T=300$ K (see Fig. 9 in Ref. 29). The frequency-independent anomaly occurred in the $\sigma(f,T)$ plot in the vicinity of 250 K.

Moreover, two frequency-independent tiny anomalies occurred also in the real part of electric permittivity $\varepsilon'(T,f)$ and the loss coefficient tan $\delta(T,f)$ dependences that could indicate a phase transition occurrence. They were visible in the vicinity of 250 K and 310–320 K. The measured effective electric permittivity $\varepsilon'(T,f)$ temperature dependence exhibited dispersion above 170 K. The partially overlapped bumplike anomalies occurred in the 200–450 K range. The broad peak with maximum shifted with frequency ($f=0.1-100$ kHz) within the wide temperature range (350–650 K). The loss coefficient temperature dependence showed the steplike anomaly in the 250–550 K range.

The most probable dielectric relaxation times are usually defined as the inverse of the frequency at the peak maximum

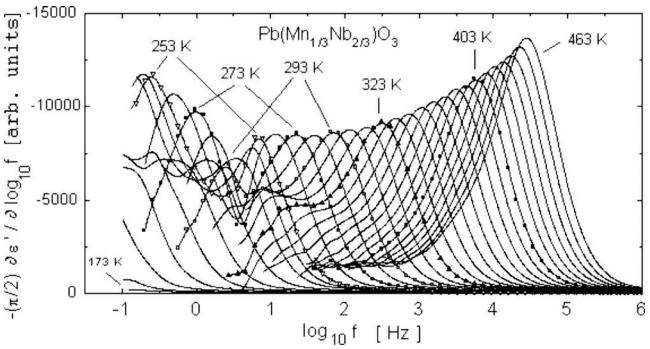

FIG. 1. The derivatives of the real part of electric permittivity $(-\pi/2)\,\partial\varepsilon'/\partial(\log_{10} f)$ vs $\log_{10} f$ plotted for the temperatures chosen with 10 K step. The isotherms obtained at 253, 273, 293, and 323 K are discerned with symbols. The coexistence of two peaks occurs in the isotherms below 323 K. The measurement carried out at ambient pressure $p=10^5$ Pa.

$$\tau_{\max} = (2\pi f_{\max})^{-1} \tag{2a}$$

in dielectric loss spectra $\varepsilon''(\omega,T)$. These relaxation times have a macroscopic meaning because they are related to macroscopic polarization decay of sample. However, the "macroscopic" relaxation times $\tau_{\max}$ relate to the "microscopic" times τ_{micro} (which correspond to Debye model dependence) with the term[37]

$$\tau_{\max} = [(\varepsilon_o + 2)/(\varepsilon_\infty + 2)]\tau_{\text{micro}}. \tag{2b}$$

Hence, the microscopic relaxation times τ_{micro} in perovskite-type oxides may be 10–100 times shorter than those determined directly from loss peaks.

The dc-conduction-free dielectric loss peaks in the $\varepsilon''(T,f)$ dependence can be received with use of the derivative

$$\varepsilon'' \approx (-\pi/2)\,\partial\varepsilon'/\partial(\log f), \tag{3}$$

since the permittivity parts $\varepsilon'(T,f)$ and $\varepsilon''(T,f)$ are interrelated by the Kramers-Kronig transforms and thus these two quantities are equivalent with respect to their information.

In case of the marked electric conduction that covers or strongly overlaps with the other relaxation process, the dielectric permittivity temperature and frequency dependences can be also analyzed with the use of the electric modulus representation, which suppresses the dc contribution

$$M^* = (\varepsilon^*)^{-1} = (\varepsilon' + i\varepsilon'')^{-1} = M' + iM''. \tag{4}$$

This approach is useful for various conducting materials such as vitreous ionic conductors[38] and polycrystalline ceramics.[39,40] From a physical point of view, the electric modulus describes the relaxation of electric field in the material sample when the electric displacement remains constant. Therefore, the modulus representation describes the real dielectric relaxation process.[41]

In case of Debye relaxation process, the relaxation times τ_M are related to the time determined from dielectric permittivity by the relation

$$\tau_{\varepsilon,\max} = [\varepsilon_0/\varepsilon_\infty]\tau_M, \tag{5}$$

which differs from Eq. (2b) by the factors "2" occurring in the numerator and the denominator. However, in case of oxide perovskite materials, which shows high values of $\varepsilon_0 \approx 10-1000$, i.e., $\varepsilon_0 \gg 2$, both relations converge. Hence, the values of relaxation times obtained from electric modulus coincide with the relaxation times in the "microscopic" meaning.

Hence, such procedure enabled us to determine the most probable relaxation times directly from position of the peak $(\tau_{\max}=1/2\pi f_{\max})$ in the $M''(T,f)$ spectrum.[29] The convex curvature of the relaxation time dependence in the Arrhenius plot (Fig. 14 in Ref. 29) indicated that the VFT law, usually applied for the analysis of the temperature dependence of structural relaxation times, could not be applied in this case.

The other possibility was the coexistence of two relaxation processes. We discerned two relaxation processes as the two limiting cases (see Fig. 14 in Ref. 29). The high-temperature range (~320–473 K) relaxation was described by activation energy $E_{M,H}=0.43$ eV and the electric conductivity characteristic relaxation time $\tau_{0,H}=1\times10^{-11}$ s. The low-temperature range (~300–173 K) relaxation was described by $E_{M,L}=0.34$ eV and $\tau_{0,L}=1\times10^{-9}$ s (see Figs. 12–14 in Ref. 29). Since the activation energy values $E_{M,L}$ compares to E_{dc}, one can point the interrelation between the relaxation processes and the electric conductivity in the $Pb(Mn_{1/3}Nb_{2/3})O_3$ ceramics.

It is worth noting that the curvature in the plots would correspond to the manifestation of the variable range hopping of small polaron mechanism of conductivity described with the term $\sigma=\sigma_0\exp[-(T_0/T)^{1/4}]$. Due to the scaling relation between the relaxation time τ and the conduction current $\sigma_{\text{dc}}=\xi/\tau$,[17] one might expect temperature relaxation times dependence would exhibit convex curvature in the Arrhenius plot.

Therefore, it was necessary to verify with use of the derivative approach whether there are two different relaxation processes or not in the $Pb(Mn_{1/3}Nb_{2/3})O_3$ ceramics. The plots obtained with the use of Eq. (3), applied for the isotherms in the 173–463 K range, are shown in Fig. 1. One peak only occurs in the $(-\pi/2)\,\partial\varepsilon'/\partial(\log_{10} f)$ vs $\log_{10} f$ dependence for the isotherms in the high-temperature range. This "high frequency" peak position moves from $f_{\text{HF}}=30$ kHz at 463 K to $f_{\text{HF}}=7$ Hz at 253 K. For the isotherms obtained below 353 K, a minor bump emerges at the lower frequencies range below ~100 Hz. For instance, one can see the coexistence of the main high frequency peak at $f_{\text{HF}}=274$ Hz and the "low frequency" bump at $f_{LT}\approx20$ Hz for the 323 K isotherm. This bump emerges to the low frequency peak for the isotherms below 323 K.

The intensities of the "high frequency" (HF) and the "low frequency" (LF) anomalies are shown in Fig. 2(a) to illustrate their evolution with temperature and frequency. When the temperature decreased, the intensity of the "HF" peak decreased. On the contrary, the intensity of the "LF" bump-like anomaly increased. When the "LF" anomaly shape changed into the peaklike shape for the isotherms below 303 K, the intensity increased with the higher rate. The "HF" and

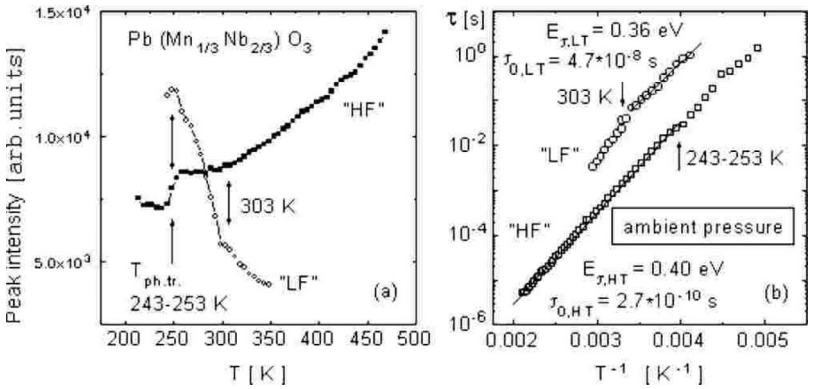

FIG. 2. (a) The intensities of the two peaks in $(-\pi/2)\partial\varepsilon'/\partial(\log_{10} f)$ isotherms. (b) The Arrhenius plot of the most probable relaxation times, τ vs T^{-1}, received from the position of the peaks in the $(-\pi/2)\partial\varepsilon'/\partial(\log_{10} f)$ isotherms. The terms "HF" and "LF" denote the "high frequency" and "low frequency" peaks, which correspond to the relaxation processes.

"LF" peaks exhibited similar intensities in case of the 283 K isotherm. The main HF peak abruptly collapsed at 243–253 K and finally smeared below 213 K. The changeover in the intensity of peaks, which occurred in vicinity of 243–253 K, may be ascribed to a phase transition.

The derivative representation $(-\pi/2)\partial\varepsilon'/\partial(\log_{10} f) \approx \varepsilon''$, applied for the ambient pressure electric data, proved the coexistence of two relaxation process. The HF and the LF relaxation dominated above and below of the phase transition, respectively. Therefore, the activation energy of relaxation and the relaxation characteristic time were determined separately in these temperature ranges [Fig. 2(b)]. The obtained values were $E_{\tau,\mathrm{HF}}$=0.40 eV and $\tau_{0,\mathrm{HF}}=2.7\times10^{-10}$ s for the HF relaxation and $E_{\tau,\mathrm{LF}}$=0.36 eV, and $\tau_{0,\mathrm{LF}}=4.7\times10^{-8}$ s for the LF relaxation. These values corresponded to the set of values determined previously with use of the modulus representation.[29] However, the derivative representation enabled us to resolve the occurrence of a phase transition, which superposed the relaxation phenomena.

B. Electric permittivity isotherm under pressure

The hydrostatic pressure applied to the $Pb(Mn_{1/3}Nb_{2/3})O_3$ ceramics, at the isothermal condition, shifted the electric permittivity dependences, $\varepsilon'(f)$ and $\varepsilon''(f)$, toward higher frequencies (Fig. 3). There were two clear bumplike anomalies visible in the $\varepsilon'(f)$ plot in the ~0.1–1 Hz and the ~100 Hz–10 kHz ranges that corresponded to the LF and the HF relaxation processes discerned in the ambient pressure measurement (compare to Fig. 12 in Ref. 29 and to Fig. 1).

With the aim to get rid of the dc conductivity participation in the spectra, the derivative was calculated with use of Eq. (3). The obtained losses $\varepsilon''(f) \approx (-\pi/2)\partial\varepsilon'/\partial(\log_{10} f)$ showed the well-resolved peak in the ~1 Hz range [Fig. 4(a)]. However, a bump-shaped anomaly occurred in the ~1 kHz range [Fig. 4(b)]. Therefore, the electric modulus imaginary part was calculated also. In this case, the clear peak appeared in the 1 kHz range [Fig. 4(c)]. The obtained peaks in the losses moved toward higher frequency with increasing pressure [see Figs. 4(a) and 4(c)]. It meant that the relaxation frequency determined for this process increased with compression. Thus, one can expect that the applied hydrostatic pressure decreased the heights of the energy barriers. Similar behavior, i.e., the decrease in the activation energy with applied pressure, was also reported for $K(TaNb)O_3$ doped with Ca ions and ascribed to a subsystem of frozen-in dipolar defects, apart from the whole lattice behavior.[42]

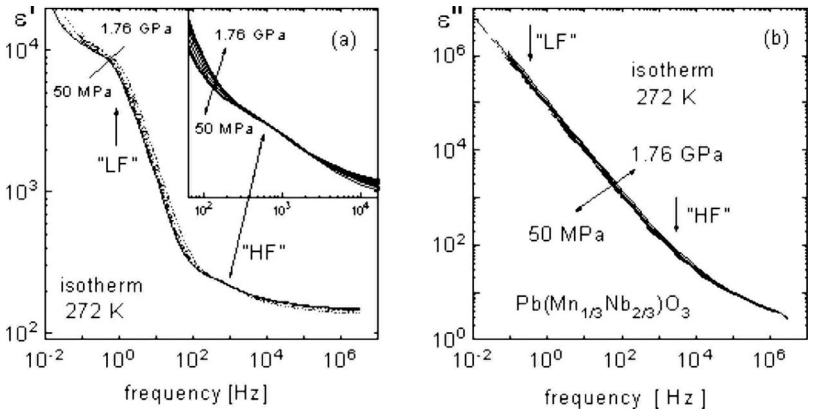

FIG. 3. The electric permittivity dependences obtained for the $Pb(Mn_{1/3}Nb_{2/3})O_3$ ceramics: (a) the real part $\varepsilon'(f,p)$, and (b) the imaginary part $\varepsilon''(f,p)$. The isothermal (T_{iso}=272 K) measurement carried out for the hydrostatic pressure changed from 50 MPa to 1.76 GPa. The arrows mark the anomalies in the low frequency range (~1 Hz) and in the high frequency range (~1 kHz).

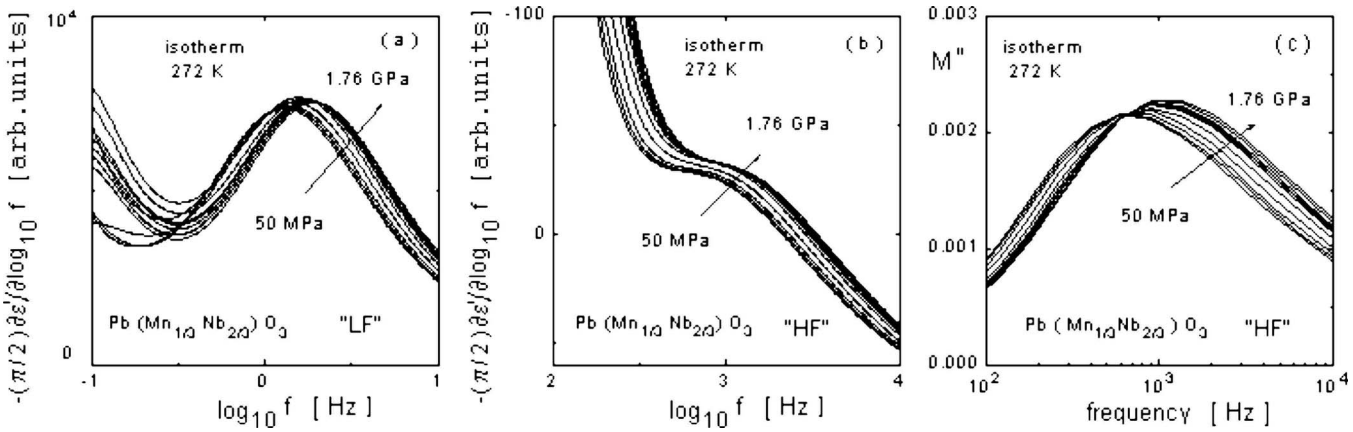

FIG. 4. The loss dependence plots obtained after procedures, which suppressed the contribution of dc conduction. The data obtained for the hydrostatic pressure changed from 50 MPa to 1.76 GPa at the isothermal conditions $T_{\mathrm{iso}}=272$ K. (a) $\varepsilon''(f,p)\approx(-\pi/2)\partial\varepsilon'/\partial(\log_{10}f)$ presented for the low frequency range. (b) $\varepsilon''(f,p)\approx(-\pi/2)\partial\varepsilon'/\partial(\log_{10}f)$ for the high frequency range. (c) The imaginary part of electric modulus $M''(f,p)$ for the high frequency range.

Moreover, it is worth noticing that such a feature of relaxation behavior is completely different from patterns of behavior usually observed for glass-forming liquids, for which compression induces the slowing of the relaxation dynamics being related to the increase in the activation energy.[43]

The electric relaxation times estimated with the use of the relation $\tau_{\max}=(2\pi f_{\max})^{-1}$ [Eq. (2a)] from the data presented in Figs. 4(a) and 4(c) are plotted in Figs. 5(a) and 5(b). In accordance to transition state theory introduced by Eyring,[44] the linear dependence of $\ln\tau$ on p can be used to define the activation volume ΔV_a:

$$\Delta V_a = RT\{\partial(\ln\tau)/\partial p\}_T. \tag{6a}$$

As it is visible in Fig. 5, the slope in the pressure dependence of $\log_{10}\tau$ changes at a crossover pressure $p_{\mathrm{cr}}\approx 0.9$ GPa both for the LF and the HF dependences. The activation law

$$\tau(p) = \tau_0 \exp[p\Delta V/RT_{\mathrm{iso}}] \tag{6b}$$

was fitted numerically in order to evaluate the activation volume ΔV_a "below" and "above" the p_{cr}. In case of the LF isotherm, the estimated values of the activation volume were $\Delta V_{a,\mathrm{below}}(\mathrm{LF})=-1.3\times10^{-30}$ m^3 and $\Delta V_{a,\mathrm{above}}(\mathrm{LF})=-0.4\times10^{-30}$ m^3. In case of the HF isotherm, the estimated values were $\Delta V_{a,\mathrm{below}}(\mathrm{HF})=-1.7\times10^{-30}$ m^3 and $\Delta V_{a,\mathrm{above}}(\mathrm{HF})=-0.5\times10^{-30}$ m^3 for the pressure range lower and higher than p_{cr}, respectively. The change of relaxation dynamics at the p_{cr}, both for the LF and the HF case, could be a manifestation of a structural transformation induced by compression.

C. Electric permittivity at high-pressure isobar

At the isobaric condition $p=1.76$ GPa, the real part of electric permittivity $\varepsilon'(T,f)$ plot moved toward higher frequencies with increasing temperature, exhibiting the "low frequency" and the "high frequency" relaxation processes (Fig. 6). The derivative of the $\varepsilon'(T,f)$ dependences was calculated with the use of Eq. (3). The obtained losses $\varepsilon''(f)\approx(-\pi/2)\partial\varepsilon'/\partial(\log_{10}f)$ showed the well-resolved peak in the LF range [1–300 Hz, Fig. 7(a)]. However, a bump-shaped anomaly occurred in the HF range [300 Hz-80 kHz, Fig. 7(b)]. Therefore, the electric modulus imaginary part was calculated also. In this case, the clear peak appeared only in the HF range [300 Hz-80 kHz, Fig. 7(c)].

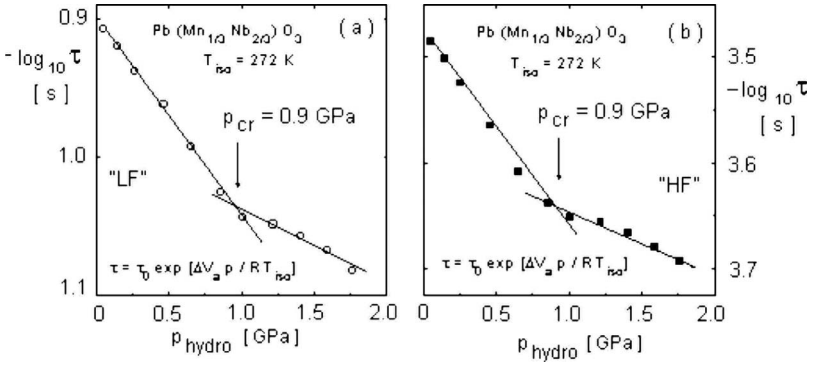

FIG. 5. The electric conductivity relaxation times $-\log_{10}\tau$ vs p plots obtained at isothermal conditions $T_{\mathrm{iso}}=272$ K. (a) The $\tau(p)$ values (o) obtained in the low frequency range from $\varepsilon''(f,p)\approx(-\pi/2)\partial\varepsilon'/\partial(\log_{10}f)$ spectrum. (b) The $\tau(p)$ values (■) obtained in the high frequency range from the electric modulus $M''(f,p)$ dependence.

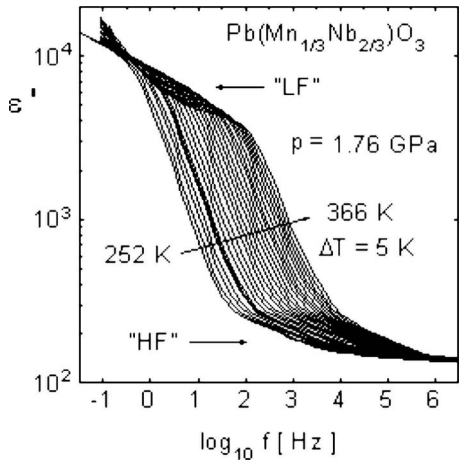

FIG. 6. The real part of electric permittivity $\varepsilon'(T,f)$ vs $\log_{10} f$ dependence. The isobar was measured at $p=1.76$ GPa at several temperatures in the 252–366 K range with the $\Delta T=5$ K step.

The most probable relaxation times evaluated [Eq. (2a)] from the loss peak in the $\varepsilon''(f,T) \approx (-\pi/2)\,\partial\varepsilon'/\partial(\log_{10} f)$ dependence [see Fig. 2(b)] were shown in Fig. 8(a) and they were ascribed to the LF relaxation process. It is visible that this dependence exhibited a slight, but clear convex curvature, i.e., neither the classical Arrhenius nor the VFT-type feature (see Fig. 11 below). Despite the slight curvature, they can be fitted in the first approximation, with the thermally activated dependence in accord to the equation

$$\tau(T) = \tau_0 \exp(E_a/k_B T), \tag{7}$$

where the activation energy $E_{a,\mathrm{LF}} \approx 0.42 \pm 0.04$ eV and the relaxation characteristic time $\tau_{0,\mathrm{LF}} \approx 1 \times 10^{-9}$ s was estimated.

In case of the high frequency relaxation process, it was possible to estimate [Eq. (2a)] the most probable relaxation times from the local extreme in the $\varepsilon''(f,T)$ steplike plots [see Fig. 7(b)]. However, due to high uncertainty of this estimation, the relaxation times were evaluated also [Eq. (2a)] from the peaks in the imaginary part of the electrical modulus $M''(f,T)$ dependence [Eq. (4)]. These two sets of data are close each other [Fig. 8(b)]. The value $E_{a,\mathrm{HF}}=0.38$ eV and $\tau_{0,\mathrm{HF}} \approx 1.1 \times 10^{-11}$ s was obtained from numerical fitting the Eq. (7) for the HF relaxation.

D. Activation energy temperature dependence

Because the relaxation times in the Arrhenius plots exhibited a slight curvature, the dependence of the activation energy on temperature was determined with the use of Eq. (8),

$$E_a = k_B\,\partial(\ln \tau)/\partial(T^{-1}), \tag{8}$$

and it was shown in Fig. 9. In case of the low frequency relaxation process [Fig. 9(a)], the $E_{a,\mathrm{LF}}(T)$ value increased from about 0.26 to 0.52 eV in the 220–300 K range for the data obtained from the ambient pressure measurement. The applied hydrostatic pressure lowered the rate of $E_{a,\mathrm{LF}}(T)$ increase. It is worth noticing that in case of the low frequency process, the activation energy increases with temperature, unlike for simple molecular glass-forming liquids. In case of the high frequency relaxation, the $E_{a,\mathrm{HF}}(T)$ dependence showed also an increase from about 0.35 to 0.42 eV in the 253–300 K range but it fluctuated ($E_{a,\mathrm{HF}} \approx 0.42 \pm 0.04$ eV) for higher temperatures. The variation in the activation energy is consistent with the local disorder related to the chemical nonhomogeneity of the $Pb(Mn_{1/3}Nb_{2/3})O_3$ ceramics.[29]

Additional effect induced by the applied pressure is visible in Fig. 9(b). For the data measured at 1.76 GPa isobaric conditions, a downward shift occurred for the $\partial(\ln \tau)/\partial(T^{-1})$ vs T dependence in comparison to data measured at ambient pressure. One can deduce that the applied hydrostatic pressure affects activation energies $E_a(T,P)$, i.e., lowers the heights of energy barriers involved in this relaxation dynamics. We have estimated the reduction in the activation energy to be about $\Delta E_{a,\mathrm{HF}} = -0.02 \pm 0.01$ eV in 252–303 K range at high-pressure conditions.

The same value of $\Delta E_{a,\mathrm{HF}} = 0.44$ eV $- 0.38$ eV $= -0.02$ eV was obtained from the average E_a values obtained from the numerical fitting to the data in the Arrhenius plots in Figs. 2(b) and 8(b). Hence, we can roughly estimate the

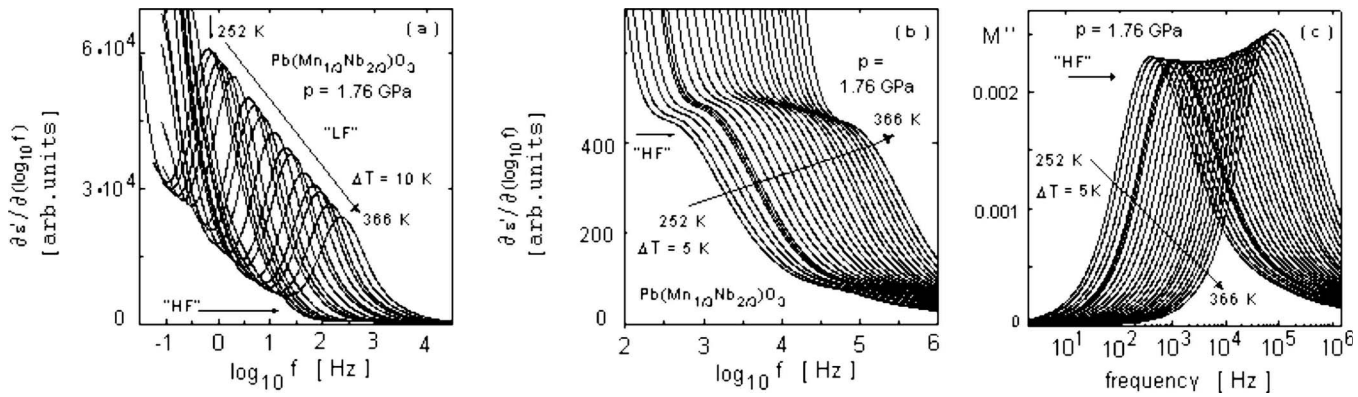

FIG. 7. The losses obtained for the $p=1.76$ GPa isobar conditions. The temperature dependent peaks correspond to the low frequency ("LF") and to the high frequency ("HF") relaxation processes. (a) The losses $\varepsilon''(f) \approx (-\pi/2)\,\partial\varepsilon'/\partial(\log_{10} f)$. The plots chosen with $\Delta T=10$ K step are shown. (b) The losses $\varepsilon''(f) \approx (-\pi/2)\,\partial\varepsilon'/\partial(\log_{10} f)$ plotted within the high frequency range at $\Delta T=5$ K step. (c) The imaginary part of electric modulus $M''(f,T,p)$, $\Delta T=5$ K step.

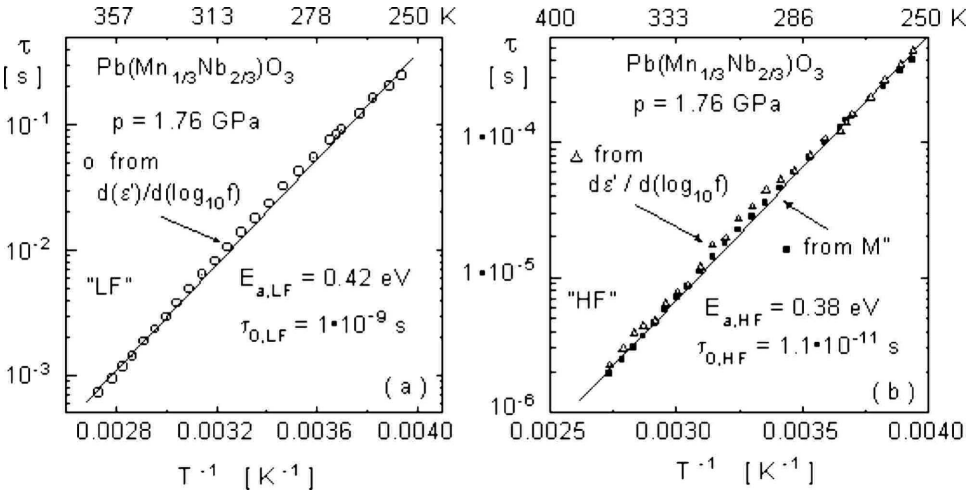

FIG. 8. (a) The relaxation times τ vs T^{-1} evaluated from the loss peak in the $\varepsilon''(f,T) \approx (-\pi/2)\,\partial\varepsilon'/\partial(\log_{10} f)$ for the low frequency process. (b) The relaxation time τ vs T^{-1} dependence obtained for the high frequency process. The data (Δ) were evaluated from the steplike anomaly in the $\varepsilon''(f,T) \approx (-\pi/2)\,\partial\varepsilon'/\partial(\log_{10} f)$ plots. The data (■) were evaluated from peaks in electric modulus $M''(f,T,p)$ plots.

pressure coefficient of the energy barrier height change as $\Delta E_{a,\mathrm{HF}}/\Delta p \cong -1$ meV kbar^{-1}. This value compares with value of −2.8 meV kbar^{-1} reported for KTN:Ca,[42] and −2 meV kbar^{-1} for PZT codoped with Bi and Ba.[45] On the other hand, the variation in activation energy with temperature in the low-temperature range ($T<300$ K) suggested a possibility other than the pure thermally activated [Eq. (7)] mechanism of relaxation.

It is known that several perovskite manganites exhibit electric conductivity described in terms of the VRH model of the small polaron that can be related to the Fermi-glass features.[19,20] Therefore, the conduction current relaxation term $\sigma_{\mathrm{dc}}=\xi/\tau$ which scales the dc conductivity to the relaxation times, $\sigma(f=0,T)\sim\omega_c\sim 1/\tau_m$, was used to determine a correspondence between temperature dependence of the relaxation times and the conductivity of the $Pb(Mn_{1/3}Nb_{2/3})O_3$ ceramics. The conductivity σ measured at ambient pressure ($p=10^5$ Pa) and at $f=100$ Hz has been plotted vs $T^{-1/4}$ in Fig. 10(a), in accordance with the following term:

$$\sigma = \sigma_0 \exp[-(T_0/T)^{1/4}], \tag{9}$$

where the parameter T_0 is related to the disorder energy which corresponds to variation in the local environment of the crystal lattice sites participating in the hopping process. This dependence is fulfilled for the $Pb(Mn_{1/3}Nb_{2/3})O_3$ sample at low-temperature range. The value of $T_{0,\sigma}=(5\pm0.4)\times10^8$ K has been obtained from the linear fit [Eq. (9)] of experimental data, carried out in the temperature range 170–240 K. Hence, it can be deduced from the temperature dependence of electric conductivity that the $Pb(Mn_{1/3}Nb_{2/3})O_3$ sample exhibited the properties of a Fermi-glass system below room temperature. In addition, a bump related to the electric conductivity relaxation process is visible in the temperature range 240–330 K. The convex curvature of $\sigma(T^{-1/4})$ plot at higher temperatures ($T>330$ K) indicates the thermally activated conductivity behavior, with E_{dc} equal to about 0.45 eV.[29]

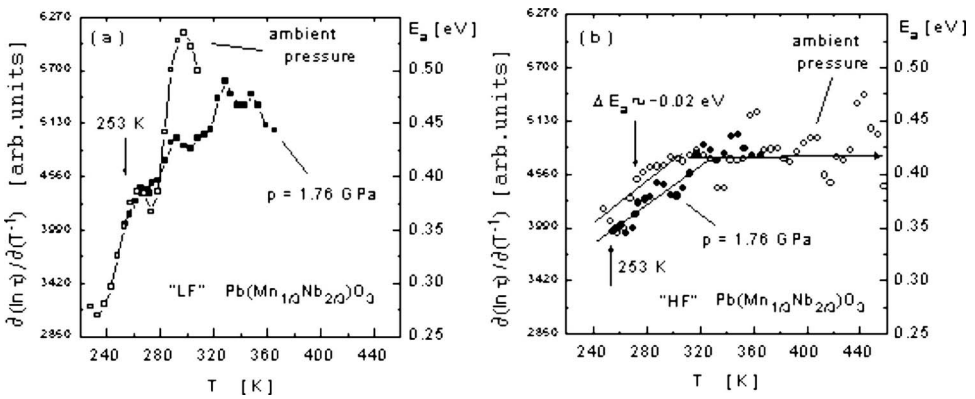

FIG. 9. The activation energy temperature dependence evaluated as $E_a(T)=\partial(\log_{10}\tau)/\partial(T^{-1})$ for the ambient pressure (□ and ○) and for the $p=1.76$ GPa (■ and ●) isobar. (a) The $E_a(T)$ obtained for the low frequency relaxation. (b) The $E_a(T)$ obtained for the high frequency relaxation. The temperature independent activation energy with value $E_a=0.42$ eV at the high-temperature range ($T>300$ K) is marked by the horizontal arrow.

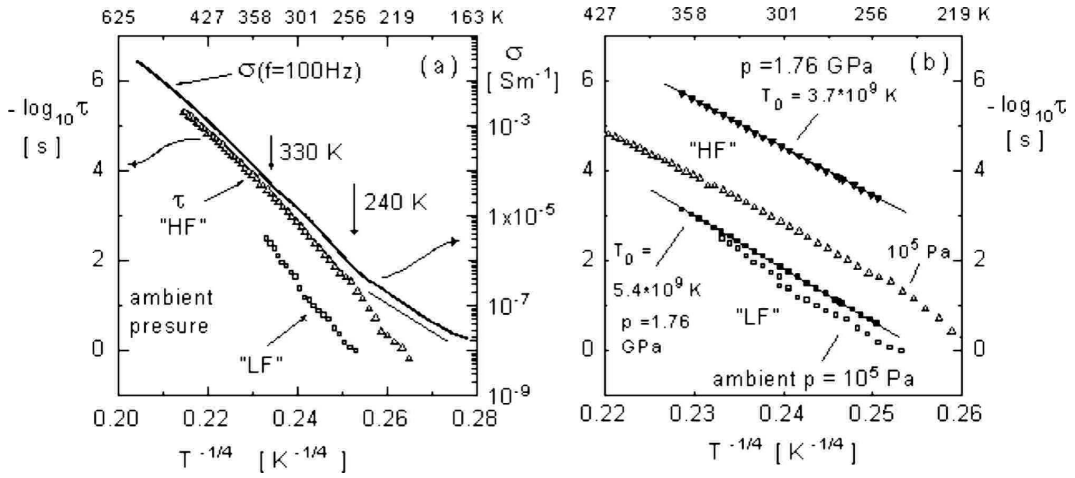

FIG. 10. (a) Temperature dependence of the electric conductivity σ vs $T^{-1/4}$, and the electric conductivity relaxation times $-\log_{10}\tau$ vs $T^{-1/4}$ obtained for the noncompressed sample. The electric conductivity and relaxation times scales in accordance to the thermally activated dependence in high-temperature range. (b) The electric conductivity relaxation times τ vs $T^{-1/4}$ obtained from the isobaric measurements: (▼) the "HF" relaxation at $p=1.76$ GPa, (△) the HF relaxation at the ambient pressure $p=10^5$ Pa, (■) the "LF" process at $p=1.76$ GPa, (□) the LF process at ambient pressure. The relaxation times temperature dependence obtained at the $p=1.76$ GPa isobar shows the Fermi-glass model features.

With the aim to test the consistency of the Fermi-glass model with the features of the relaxation dynamic, the relaxation times obtained in the case when the $Pb(Mn_{1/3}Nb_{2/3})O_3$ sample was not compressed (ambient pressure, $p=10^5$ Pa) were also plotted in Fig. 10(a), in accordance with the term

$$\tau(T) = \tau_0 \exp[(T_0/T)^{1/4}]. \quad (10)$$

In case of the high frequency relaxation, the $-\log_{10}\tau(T^{-1/4})$ dependence showed also the convex curvature in the high-temperature range ($T>240$ K). Therefore, agreement between the temperature behavior of the relaxation times $\tau(T^{-1/4})$ and the electric conductivity $\sigma(T^{-1/4})$ proved that the temperature dependence of the high frequency relaxation times scales to the electric conductivity at high temperatures.

In contrary, the dependence of the HF relaxation times in a temperature range below the phase transition ($T<240$ K) was vague. Similarly, the LF relaxation times in its whole temperature range (243–353 K) was not clear enough to verify the conduction current relaxation term $\sigma=\xi/\tau$.

In case of the compressed $Pb(Mn_{1/3}Nb_{2/3})O_3$ sample ($p=1.76$ GPa), the $T^{-1/4}$ temperature dependence of the relaxation times was fitted with high accuracy using Eq. (10) [Fig. 10(b)]. For the LF relaxation process $T_{0,\tau LF}=(5.4\pm0.2)\times10^9$ K was evaluated. Similarly, for the HF process the value $T_{0,\tau HF}=(3.7\pm0.2)\times10^9$ K was obtained. It would be mentioned that the LF data were obtained from derivative procedure [Eq. (3)] and the HF data from the electric modulus approach [Eq. (4)].

Hence, the Fermi glasslike features were stabilized under the high-pressure conditions within this entire temperature range (252–366 K) where the low and high frequency relaxation times were estimated [compare Figs. 7, 8, and 10(b)]. On the other hand, they were observed within higher temperature range in comparison to the temperature range, where such properties of conductivity of the noncompressed sample (below 240 K) occurred. Therefore in consequence the conduction current relaxation term $\sigma=\xi/\tau$ for the Fermi glass could not be directly confirmed.

IV. DISCUSSION

There are several models that deal with the mixed contribution of mobile ions and polarons to the electric conduction and relaxation. The dynamics of the ions can be described within the concepts of mismatch and relaxation,[46] and migration model[47] developed from jump relaxation models where the ions are hopping over a barrier back and forth between nearby vacant sites. Additionally, the jump relaxation model is not contradictory to the polaronic conductivity at high temperatures.[48] On the other hand, polaronic conductivity in the glassy systems at low temperatures may be described within the VRH model, where electrons or polarons are localized nearby Fermi energy levels.[17,18,20]

As showed schematically in Fig. 11, various patterns of temperature dependence of $\tau(T^{-1})$ could be observed for disordered systems. These are depicted as follows. The straight line for the Arrhenius dependence in case of pure Debye relaxation, the concave curve for the VFT-type behavior, and the convex curve for the Fermi-glass model. Such discrimination enables us to discern the dominating relaxation mechanism directly from the temperature dependence of measured relaxation times.

From the microscopic point of view, the Gate model can describe the dynamics of ions in defected or disordered materials.[16,49–52] This model includes into activation energy both strain energy and electrostatic binding energy. It give us a possibility to test whether the observed effects can be adequately described as the pressure influence on the potential energy barrier.

The heterovalence metal ions, substituted into the host, usually form dipolelike Me-V_O pairs, which relax by reorientation. Such effects may by a dominant relaxation process.

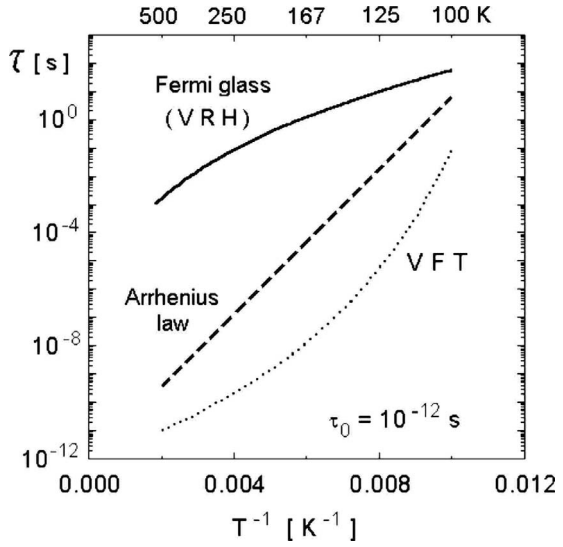

FIG. 11. The schematic picture of different temperature dependences of the relaxation times, τ vs T^{-1}, observed in disordered systems. The dashed line represents the Arrhenius law, valid, e.g., for pure Debye relaxation, the line with concave curvature depicts the VFT behavior, and the convex curvature line shows the case of the Fermi-glass model.

In the case when the defects introduce energy levels lower than 1 eV, semiconductor properties and effects originating from thermal activation of charge carriers may occur in such materials and can produce additional electrical losses. It is worth noticing that the space charges and the lattice responses are visible as separate processes and can be described with the use of two Cole-Cole relaxation functions.[53]

In the doped perovskites, a relaxation process related to dipoles originating from point defects subsystem can be distinguished as the additional process, which contributes to the overall electric permittivity. Such examples for two types of coexisting relaxation processes, i.e., one proceeding in a defects subsystem and the other related to the ferroelectric or relaxor phase transition, were reported for e.g., $K(Ta,Nb)O_3:Mn$,[42] $K(Ta,Nb)O_3:Ca$,[42] $Pb(Zr,Ti)O_3$ codoped with Ba and Bi ions,[45] and in $Ba(Ti,Zr)O_3$.[36]

We assume that the electric properties of $Pb(Mn_{1/3}Nb_{2/3})O_3$ ceramics studied under hydrostatic pressure can be related to dipolelike defects subsystem. Application of hydrostatic pressure results in effects as follows: (a) the relation known as the "conduction current relaxation" which links the temperature dependence of electrical current conduction and relaxation times, (b) the occurrence of crossover pressure p_{cr}, (c) the applicability of the Gate model in case of the strain-dependent activation energy related to $V_{Mn/Nb}$ bivacancy, and (d) the decrease in the activation energy induced by applied high pressure.

A. Conduction current relaxation

The relaxation process in the $Pb(Mn_{1/3}Nb_{2/3})O_3$ ceramics is related to small polaron hopping mechanism that is determined by the potential barriers. It has been shown that both the electric conductivity and high frequency ($f \sim 1$ kHz) relaxation times behave in the high-temperature range in accordance to the thermally activated behavior of small polaron [see Fig. 9 in Ref. 29 and Figs. 8(b) and 10(a)]. Therefore, the conduction current relaxation term $\sigma = \xi/\tau$ scales the dc conductivity to the HF relaxation times: $\sigma(f,T) \sim \omega_c \sim 1/\tau_m$, where $\sigma_{dc} \propto (T/T_0)^q (e^2/kT)\omega_c$, and $\sigma_{dc} = \sigma_{0,dc} \exp[-(E_{dc}/k_B T)]$.

The correspondence between the electric conduction and relaxation times in the low-temperature range is vague. The electric conduction shows the temperature dependence characteristic for the Fermi-glass system that is consistent with the spatial variation in the energy barriers distribution in the sample. Such behavior originated from the chemical disorder, the local imbalance of electrical charges, and also influenced by local stresses and strains occurring in the vicinity of point defects that implied occurrence of the Fermi glass.[16,54,55]

The variation in the barrier heights $E_a(T)$ was deduced also from the relaxation times temperature dependence in case of the low frequency ($f \sim 1$ Hz) relaxation, i.e., from the $1/\tau_m \sim \omega_c = \omega_{ph} \exp[-(T_0/T)^{1/4}]$ dependence. This feature is enhanced by application of hydrostatic pressure. However, both the incompatibility of the respective temperature ranges and the overlapping of phase transition effects observed at ambient pressure caused the scaling within the Fermi-glass model remained uncertain.

B. Crossover pressure occurrence

It has been shown that the Mn^{k+} ions replacing the Nb ions induce local strain u_d, which can be estimated from the crystal radii. The strain u_d, at the distance relatively long $r = 1$ nm, occurring around the Mn^{k+} ions ($k=2, 3, 4$) are on the order of 10^{-4} and the associated stresses, $\sigma_d = Cu_d$, vary on several MPa levels.[14] The stresses occurring in the vicinity of Mn ions are comparable to the mismatch stresses occurring at boundaries between nonhomogeneities occurring in the perovskite host lattice of the investigated material. Moreover, they are much weaker than observed crossover pressure, $p_{cr} \approx 0.9$ GPa. Similarly, strains, which appear due to aging effects related to domain structure and migration of space charge, were calculated as varying on MPa level.[56] Therefore, the applied hydrostatic pressure of 1.76 GPa is able to induce a structural transformation in such a locally deformed crystal lattice.

C. Gate model for strain-dependent activation energy

We assumed that pressure-dependent activation energy would be ascribed to a stress-strain effect. Hence, we searched for a microscopic mechanism, which could be used for description of such relaxation effects. We have presumed that: (1) the Mn ions change their valence states, (2) the bivacancies V_O-$V_{Mn/Nb}$ participate in the ion hopping and the relaxation, (3) the quantitative description can be carried out with use of the Gate model since pressure affects primarily ionic behavior, and (4) role of the Mn ions or Mn-V_O centers in the relaxation should be verified.

In the case of the $Pb(Mn_{1/3}Nb_{2/3})O_3$ material the relaxation process is pressure sensitive. The applied pressure sta-

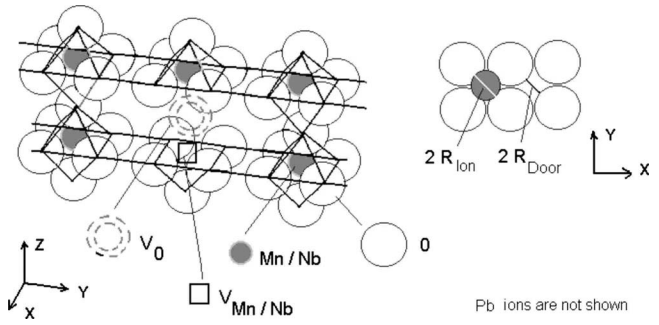

FIG. 12. Schematic image of the octahedra network for $Pb(Mn_{1/3}Nb_{2/3})O_3$ compound. The Pb ions, placed outside the octahedra, are not drawn for clarity. The picture in the left side of the figure shows two square pyramids formed in the vicinity of oxygen vacancy. The picture in the right side shows relations between the oxygen, Mn or Nb, and the "doorway" radii.

bilizes the Fermi-glass properties, which are related to polaronic mechanism of conductivity. On the other hand, the values of the electric conductivity relaxation characteristic times $\tau_{0,LF} \sim 10^{-8}-10^{-9}$ s, and $\tau_{0,HF} \sim 10^{-10}-10^{-11}$ s (obtained for the LF and the HF relaxation at ambient pressure and at $p=1.76$ GPa, respectively) suggest ionic mechanism of this relaxation.

Participation of oxygen vacancies in the electric conduction and relaxation is generally accepted in literature, due to their role as the source of thermally generated electrons[57] and as the background for oxygen ions hopping at high temperatures, respectively. The hopping of oxygen ions in perovskite structure proceeds to nearest-neighbor vacancies. We would like to mention that in case of similar Mn-containing compound, i.e., $(Na_{0.75}Bi_{0.25})(Mn_{0.25}Nb_{0.75})O_3$, the electric conductivity relaxation process, occurring below 440 K with activation energy about 0.4 eV, has been identified.[40]

The manganese ions Mn^{k+}, with $k=2$, 3, and 4, can coexist in manganite-based compounds,[29,58–61] since these states are stabilized by neighboring heterovalence ions or oxygen vacancies. We assume that the Mn^{3+} ions are stable at low temperature, and the change in Mn ion valence occurs on heating,

$$Mn^{3+} \rightarrow Mn^{4+} + e^{-}. \tag{11}$$

The thermally activated electrons can participate in conduction, which actually occurs as the mixed electronic-ionic type. On the other hand, the change in Mn valence corresponds to the decrease in ionic radius of Mn ion. Therefore complex of combined charge and stress effects ought to influence the unit cell parameters and electronic structure.

Since we consider the hopping and relaxation of Mn and/or Nb ions, an available pathway for such movement should be proposed. The Mn and Nb ions are the 3*d* and 4*d* ions, respectively, and from a stereo-chemical point of view their octahedral coordination MnO_6 or NbO_6 is expected. However, occurrence of an oxygen vacancy leads, in consequence, to formation of square-based pyramids MnO_5 or NbO_5 in perovskite-derived structures of manganites.[62] Within such structures, the Mn and/or Nb ion can jump into a vacancy $V_{Mn/Nb}$, which is placed in the next-nearest-neighbor position in the proper sublattice. Since the perovskite structure is dense, the effective Mn ion hopping is possible via an oxygen vacancy placed in between (Fig. 12). Therefore, we assume that the bivacancy V_O-$V_{Mn/Nb}$ participates in the hopping of Mn or Nb ions from one square-based pyramid to the other.

The $Pb(Mn_{1/3}Nb_{2/3})O_3$ ceramics shows deformed multiple unit cells with monoclinic symmetry.[29] The pseudocubic representation of these monoclinic cell parameters is $a_{pc}=6.126$ Å, which may reflect the cluster of the BO_6 octahedron (with ridge dimension about 4 Å, resembling a perovskite unit cell) and the square-pyramid BO_5.

To describe the process of Mn/Nb ions jumping to the $V_{Mn/Nb}$ vacancies, we consider the pressure effects with use of the Gate model.[16,49,50] According to this model, the potential energy barrier E_a consists of strain energy ΔE_S and electrostatic binding energy ΔE_B. The evaluation of the strain energy contribution in the case of the Mn and Nb ions is presented below. The comparison of the activation energy obtained from the electric conductivity and electric modulus analysis will allow us to identify the most probable microscopic mechanism involved in the relaxation dynamics.

In the case when the strain energy is related to elastic energy required to dilating necessary space for the ionic jumping, the ΔE_S is expressed by the term[49]

$$\Delta E_S = 4\pi G R_{door}(R_{ion} - R_{door})^2, \tag{12}$$

where G is shear modulus, R_{ion} is radius of the mobile ion, and R_{door} denotes the "doorway" radius when the mobile ion has to push the surrounding ions away while it hops to another place.

The R_{door} has been evaluated as the distance between oxygen ions, estimated diagonally in the pyramid base (see Fig. 12),

$$R_{door} = D - d_{O\text{-}O} = \sqrt{2}(2R_O) - (2R_O). \tag{13}$$

The distance $d_{O\text{-}O}$ has been taken as equal to the ridge in the pyramid base, in spherical approximation, i.e., $d_{O\text{-}O}=2R_O \approx 2.8$ Å gives $R_{door} \approx 0.55$ Å. This value is smaller than both Mn^{k+} and Nb^{5+} radii (in 6nn coordination, after Shannon,[63] see Table I).

The exact experimental value of shear modulus for the $Pb(Mn_{1/3}Nb_{2/3})O_3$ ceramics samples remains unknown and thus the effective value of Young's modulus $C=117$ GPa was used to obtain an approximate G value. The bulk modulus K and elastic constants are related by expression $K=(3\lambda+2\mu)/3$. In many cases $\lambda=\mu$ and thus the shear modulus can be approximated by $G \approx \mu \approx (3/5)K$.[15] One can find also other estimations, e.g., relation between the Young's and the shear modulus that for several glasses is taken as $G \approx 0.4C$.[49] Therefore, the evaluation of the strain energy value for studied ceramics has been carried out using two estimations, i.e., $G_1=(3/5)C$, and $G_2=0.4C$, considered as two limiting cases. Values of ΔE_{S1} and ΔE_{S2} obtained with use of Eq. (12) are shown in Table I.

In the case when the ΔE_S is related to the distance of the jump L_{jump}, the modified expression is written as[51,52]

$$\Delta E_{S,jump} = \pi G L_{jump}(R_{ion} - R_{door})^2. \tag{14}$$

TABLE I. Strain energy ΔE_S values obtained within Gate model where V_O-$V_{Mn/Nb}$ bivacancy is presumed and the Mn or Nb ions jump to $V_{Mn/Nb}$ site via oxygen vacancy V_O. The ionic radii R_{ion} of the mobile ions are taken for six nearest-neighbor coordination (Ref. 63). The R_{door} denotes the "doorway" radius calculated from radii of oxygen ions, which form the pyramid base. The ΔE_{S1} and ΔE_{S2} have been evaluated with use of Eq. (12) (Refs. 16 and 49). The $\Delta E_{S1,jump}$ and $\Delta E_{S2,jump}$ have been evaluated with use of Eq. (14) (Refs. 51 and 52). Shear modulus G values were estimated as $G_1 \approx \frac{1}{2}C$ and $G_2 \approx (3/5)C$, where effective Young's modulus $C=117$ GPa has been estimated by comparison with nanoindentation test made in Hysitron Laboratory on similar compound, i.e., $Bi(Mn_{1/3}Nb_{2/3})O_3$ ceramics.

Mobile ion	R_{ion} (Å)	R_{door} (Å)	$R_{door}-R_{ion}$ (Å)	G_1 (GPa)	ΔE_{S1} (eV)	G_2 (GPa)	ΔE_{S2} (eV)	L_{jump} (Å)	G_1 (GPa)	$\Delta E_{S1,jump}$ (eV)	G_2 (GPa)	$\Delta E_{S2,jump}$ (eV)
Mn^{2+}	0.97	0.55	0.42	70	0.85	47	0.57	4.0	70	1.55	47	1.04
Mn^{3+}	0.79	0.55	0.24	70	0.28	47	0.19	4.0	70	0.50	47	0.34
Mn^{4+}	0.67	0.55	0.12	70	0.07	47	0.05	4.0	70	0.12	47	0.08
Nb^{5+}	0.78	0.55	0.23	70	0.26	47	0.17	4.0	70	0.47	47	0.31

The values $\Delta E_{S,jump}$ obtained from Eq. (14) for both shear modulus, G_1 and G_2 and the L_{jump} taken as 4 Å are also collected in Table I. These values are markedly higher in comparison to those calculated with use of Eq. (12).

As it was mentioned above, according to the Gate model assumption, the activation energy of ionic conduction consists of the binding and the strain parts. The reasonable value of strain ΔE_S should be lower than activation energy values $E_{\tau,LF}=0.36-0.42$ eV and $E_{\tau,HF}=0.38-0.40$ eV obtained from $\varepsilon''(f,T)$ or $M''(T,f)$ dependences, i.e., obtained for the LF and the HF relaxation, respectively. They should be also lower than $E_{dc,1}=0.45$ eV and $E_{dc,2}=0.34$ eV obtained from $\sigma(T)$ measured at ambient pressure.

The most probable mechanism of ionic jumping involved in relaxation process is deduced for the Mn^{4+} ions participation, for which value $\Delta E_S=0.05-0.12$ eV have been estimated as the lowest for the all considered cases (see Table I), due to smallest radius of the Mn^{4+} ion. Participation of the Mn^{3+} and the Nb^{5+} ions is less probable. The participation of the large Mn^{2+} ion is improbable in the framework of considered relaxation model because the values of ΔE_S, estimated both with the use of Eqs. (12) and (14), were too high in the case (see Table I).

The results, obtained for the studied $Pb(Mn_{1/3}Nb_{2/3})O_3$ compound, show that the relaxation, which occurs at high temperatures, can be reasonably described by the Gate model. Therefore, the Mn ion jumping and relaxation between the square-pyramid oxygen cages, via the linking oxygen vacancy, may be considered as an alternative for the alone oxygen ion jumping to oxygen vacancy and relaxation.

D. Activation energy shift

The applied external hydrostatic pressure modifies the distribution of barrier heights, which affects the high frequency relaxation process. This effect can be described by the elastic component of enthalpy, which is introduced into the relation, which described dependence of the relaxation times,

$$\tau(T) = \tau_0 \exp[(E_a - \sigma u \Delta V_{a,loc})/k_B T]. \quad (15)$$

It is worth mentioning that the $Pb(Mn_{1/3}Nb_{2/3})O_3$ ceramics are not ferroelectric. Hence, pressure influences dielectric properties due to electrostrictive effects, and the linear spontaneous polarization (piezoelectric term) in the enthalpy is omitted.[13,14,16,54]

The applied hydrostatic pressure decreased the activation energy [see Figs. 2(b), 8(b), and 9(b)] and the difference $\Delta E_a=E_a(10^5$ Pa$)-E_a(1.76$ GPa$)$ was equal about -0.02 eV. This shift in the value of the activation energy can be described in terms of the local stresses σ, and strains u, which occur in the disordered crystal lattice, $\Delta E_a=\sigma u \Delta V_a$. The evaluation of the volume $\Delta V_{a,loc} \approx -0.7\times10^{-30}$ m^3 related to the $\Delta E_a=-0.02$ eV can be made using the Young's modulus value $C=117$ GPa, since $\sigma u=p^2/C=3\times10^7$ Nm^{-2} for the applied $p=1.76$ GPa. This $\Delta V_{a,loc}$ value is comparable to the activation volume $\Delta V_{a,below}(HF) \approx -1.7\times10^{-30}$ m^3 and $\Delta V_{a,above}(HF) \approx -0.5\times10^{-30}$ m^3 obtained from the $\tau(p)$ dependence for the HF process [see Fig. 5(b)].

Moreover, the applied hydrostatic pressure affected also the low frequency relaxation at isothermal conditions [see Fig. 5(a)]. The effects can be described similarly due to close change in the activation volume, which decreased from $\Delta V_{a,below}(LF) \approx -1.3\times10^{-30}$ m^3 to $\Delta V_{a,above}(LF) \approx -0.4\times10^{-30}$ m^3.

The $\Delta V_{a,loc}$ is much smaller than the elementary cell volume $V_{cell} \approx 64\times10^{-30}$ m^3 in the perovskites, hence, the evaluated activation volume $\Delta V_{a,loc}$ can be treated as the deformed fraction of the unit cell or the unit cell deformation caused by the external pressure. It should be mentioned that the magnitude of the ratio $\Delta V_{a,loc}/V_{cell} \approx 1\%$ seems to be reasonable.[64]

V. CONCLUSIONS

It may be briefly summarized that for electrical properties of the $Pb(Mn_{1/3}Nb_{2/3})O_3$ ceramics, (1) the low frequency and the high frequency relaxation processes were separated, (2) the stress-strain effects influence distribution of the barrier heights, (3) the Fermi-glass phase features are enhanced by the applied hydrostatic pressure, and (4) the microscopic model which joined the change in Mn valence state, the bivacancy V_O-$V_{Mn/Nb}$ occurrence, and the Gate model, was proposed to describe the mixed ionic-polaronic mechanism of electric conduction relaxation.

ACKNOWLEDGMENTS

The financial support from the Committee for Scientific Research, Poland KBN under Grant No. 1P03B 075 28 is gratefully acknowledged. The authors thank Hysitron Laboratory for determination of Young's modulus value with use of nanoindentation test on $Bi(Mn_{1/3}Nb_{2/3})O_3$ ceramics [Sample Analysis Report (Doc. NRL-D-214)].

*Corresponding author; andrzej.molak@us.edu.pl. FAX: +48(32) 2588431.

[1] A. K. Jonscher, J. Phys. D **13**, L89 (1980).
[2] M. D. Ediger, C. A. Angell, and S. R. Nagel, J. Phys. Chem. **100**, 13200 (1996).
[3] M. Paluch, C. M. Roland, and S. Pawlus, J. Chem. Phys. **116**, 10932 (2002).
[4] E. L. Venturini, G. A. Samara, and W. Kleemann, Phys. Rev. B **67**, 214102 (2003).
[5] G. Singh, V. S. Tivari, and V. K. Wadhawan, Solid State Commun. **129**, 665 (2004).
[6] A. A. Bokov and Z.-G. Ye, J. Mater. Sci. **41**, 31 (2006).
[7] G. A. Samara, J. Phys.: Condens. Matter **15**, R367 (2003).
[8] R. Pirc, R. Blinc, and V. Bobnar, Phys. Rev. B **63**, 054203 (2001); R. Blinc, V. Bobnar, and R. Pirc, *ibid.* **64**, 132103 (2001).
[9] H. Vogel, Phys. Z. **22**, 645 (1921); G. S. Fulcher, J. Am. Ceram. Soc. **8**, 339 (1925); G. Tammann and W. Hesse, Z. Anorg. Allg. Chem. **156**, 245 (1926).
[10] C. M. Roland, S. Hensel-Bielowka, M. Paluch, and R. Casalini, Rep. Prog. Phys. **68**, 1405 (2005).
[11] K. Gesi, Phase Transitions **40**, 187 (1992).
[12] G. A. Samara, Solid State Phys. **56**, 239 (2001); G. A. Samara and E. L. Venturini, Phase Transitions **79**, 21 (2006).
[13] A. R. Freeman and S. P. Joshi, Ferroelectrics **227**, 1 (1999).
[14] A. Molak, J. Phys.: Condens. Matter **13**, 9561 (2001).
[15] J.-P. Poirier, *Introduction to the Physics of the Earth's Interior* (Cambridge University Press, Cambridge, 1991), Chap. 6.
[16] J. Kawamura, R. Asayama, N. Kuwata, and O. Kamishima, in *Physics of Solid State Ionics*, edited by T. Sakuma and H. Takahashi (Res Sighpost, Kerala, India, 2006).
[17] A. Hunt, Solid State Commun. **80**, 151 (1991); J. Phys.: Condens. Matter **3**, 7831 (1991); A. G. Hunt, Philos. Mag. B **81**, 875 (2001).
[18] N. F. Mott and E. A. Davies, *Electronic Processes in Non-Crystalline Materials* (Clarendon, Oxford, 1971), Chaps. 2 and 7.
[19] Y. Sun, X. Xu, and Y. Zhang, J. Phys.: Condens. Matter **12**, 10475 (2000).
[20] A. Banerjee, S. Pal, E. Rozenberg, and B. K. Chaudhuri, J. Phys.: Condens. Matter **13**, 9489 (2001); S. Pal, A. Banerjee, E. Rozenberg, and B. K. Chaudhuri, J. Appl. Phys. **89**, 4955 (2001).
[21] A. Molak, M. Paluch, S. Pawlus, Z. Ujma, M. Pawelczyk, and I. Gruszka, Phase Transitions **79**, 447 (2006).
[22] C. Godet, J. Non-Cryst. Solids **299-302**, 333 (2002).
[23] K. K. Som and B. K. Chaudhuri, Phys. Rev. B **41**, 1581 (1990).
[24] G. A. Samara, W. F. Hammetter, and E. L. Venturini, Phys. Rev. B **41**, 8974 (1990).
[25] R. Pelster, G. Nimtz, and B. Wessling, Phys. Rev. B **49**, 12718 (1994).
[26] O. Chauvet, T. Stoto, and L. Zuppiroli, Phys. Rev. B **46**, 8139 (1992).
[27] J. Modlich, O. Jarchov, T. Rentschler, A. Reller, and U. Bismayer, Solid State Ionics **95**, 131 (1997).
[28] I. H. Brunskill, R. Boutellier, W. Depmeier, and H. Schmid, J. Cryst. Growth **56**, 541 (1982).
[29] A. Molak, E. Talik, M. Kruczek, M. Paluch, A. Ratuszna, and Z. Ujma, Mater. Sci. Eng., B **128**, 16 (2006).
[30] S. Sharma, R. N. P. Choudary, and R. Sati, J. Mater. Sci. Lett. **12**, 530 (1993).
[31] B.-Sh. Li, G.-R. Li, Q.-R. Yin, Z.-G. Zhu, A.-L. Ding, and W.-W. Cao, J. Phys. D **38**, 1107 (2005).
[32] Ch.-S. Chen, Chi.-H. Hsu, and Ch.-Ch. Chou, Integr. Ferroelectr. **53**, 489 (2003).
[33] H. Chen, X. Guo, and Zh. Meng, Mater. Chem. Phys. **75**, 202 (2002).
[34] N. Ichinose and K. Yamaguchi, Ferroelectrics **158**, 307 (1994).
[35] J. Ryu, Sh. Priya, Ch. Sakaki, and K. Uchino, Jpn. J. Appl. Phys., Part 1 **41**, 6040 (2002).
[36] A. A. Bokov, M. Maglione, and Z.-G. Ye, J. Phys.: Condens. Matter **19**, 092001 (2007).
[37] Ch. P. Smyth, in *Dielectric Behavior and Structure, International Chemical Series*, edited by L. P. Hammett (McGraw-Hill, New York, 1955).
[38] P. B. Macedo, C. T. Moynihan, and R. Bose, Phys. Chem. Glasses **13**, 171 (1972).
[39] J. Liu, Ch.-G. Duan, W.-G. Yin, W. N. Mei, R. W. Smith, and J. R. Hardy, J. Chem. Phys. **119**, 2812 (2003).
[40] A. Molak, M. Paluch, S. Pawlus, J. Klimontko, Z. Ujma, and I. Gruszka, J. Phys. D **38**, 1450 (2005).
[41] H. Wagner and R. Richert, Polymer **38**, 5801 (1997); C. Leon, M. L. Lucia, and J. Santamaria, Phys. Rev. B **55**, 882 (1997); R. Richert and H. Wagner, Solid State Ionics **105**, 167 (1998).
[42] G. A. Samara and L. A. Boatner, Phys. Rev. B **61**, 3889 (2000).
[43] M. Paluch, A. Patkowski, and E. W. Fischer, Phys. Rev. Lett. **85**, 2140 (2000).
[44] H. Eyring, J. Chem. Phys. **3**, 107 (1935).
[45] G. A. Samara, Phys. Rev. B **71**, 224108 (2005).
[46] K. Funke, R. D. Banhatti, S. Brueckner, C. Cramer, C. Krieger, A. Mandanici, C. Martiny, and I. Ross, Phys. Chem. Chem. Phys. **4**, 3155 (2002).
[47] K. Funke and R. D. Banhatti, Solid State Ionics **177**, 1551 (2006).
[48] K. Funke, C. Kramer, B. Roling, T. Saatkamp, D. Wilmer, and M. D. Ingram, Solid State Ionics **85**, 293 (1996).
[49] O. L. Anderson and D. A. Stuart, J. Am. Ceram. Soc. **37**, 573 (1954).
[50] Y. Oyama and J. Kawamura, Solid State Ionics **53-56**, 1221 (1992).
[51] T. Ishii, J. Phys. Soc. Jpn. **61**, 2002 (1992).
[52] W. Yao and S. W. Martin, Solid State Ionics **178**, 1777 (2008).

[53] D. Ming, J. M. Reau, J. Ravez, J. Gitae, and P. Hagenmuller, J. Solid State Chem. **116**, 185 (1995).
[54] A. E. Glazounov, A. K. Tagantsev, and A. J. Bell, Phys. Rev. B **53**, 11281 (1996).
[55] F. Henn, S. Devautour, L. Maati, J. C. Giuntini, H. Schaefer, J. V. Zanchetta, and J. Vanderschueren, Solid State Ionics **136-137**, 1335 (2000).
[56] D. C. Lupascu, Y. A. Genenko, and N. Balke, J. Am. Ceram. Soc. **89**, 224 (2006); Y. A. Genenko and D. C. Lupascu, Phys. Rev. B **75**, 184107 (2007).
[57] S. A. Prosandeyev, N. M. Teslenko, and A. V. Fisenko, J. Phys.: Condens. Matter **5**, 9327 (1993).
[58] A. Molak and J. Kubacki, Cryst. Res. Technol. **36**, 893 (2001); J. Kubacki, A. Molak, and E. Talik, J. Alloys Compd. **328**, 156 (2001).
[59] A. Molak, Solid State Commun. **62**, 413 (1987).
[60] A. Wolska, A. Molak, K. Ławniczak-Jabłońska, J. Kachniarz, E. Piskorska, I. N. Demchenko, I. Gruszka, and D. W. Lindle, Phys. Scr., T **115**, 989 (2005).
[61] J. M. Alonso, J. M. Gonzalez-Calbet, A. Hernando, M. Vallet-Regi, M. E. Davila, and M. C. Asensio, J. Phys. Chem. Solids **67**, 571 (2006).
[62] C. Bougerol, M. F. Gorius, and I. E. Grey, J. Solid State Chem. **169**, 131 (2002).
[63] R. D. Shannon, Acta Crystallogr., Sect. A: Cryst. Phys., Diffr., Theor. Gen. Crystallogr. **32**, 751 (1976).
[64] M. Friak, A. Schindlmayr, and M. Scheffler, New J. Phys. **9**, 5 (2007).